Time domain simulation of Gd^{3+}-Gd^{3+} distance measurements by EPR

Nurit Manukovsky[1], Akiva Feintuch[1], Ilya Kuprov[2], and Daniella Goldfarb[1]

[1]Department of Chemical Physics, Weizmann Institute of Science, Rehovot 7610001, Israel

[2]School of Chemistry, University of Southampton, Southampton, SO17 1BJ, UK

ABSTRACT

Gd^{3+}-based spin labels are useful as an alternative to nitroxides for intramolecular distance measurements at high fields in biological systems. However, double electron-electron resonance (DEER) measurements using model Gd^{3+} complexes featured a low modulation depth and an unexpected broadening of the distance distribution for short Gd^{3+}-Gd^{3+} distances, when analysed using the software designed for S=1/2 pairs. It appears that these effects result from the different spectroscopic characteristics of Gd^{3+} – the high spin, the zero field splitting (ZFS), and the flip-flop terms in the dipolar Hamiltonian that are often ignored for spin-1/2 systems. An understanding of the factors affecting the modulation frequency and amplitude is essential for the correct analysis of Gd^{3+}-Gd^{3+} DEER data and for the educated choice of experimental settings, such as Gd^{3+} spin label type and the pulse parameters.

This work uses time-domain simulations of Gd^{3+}-Gd^{3+} DEER by explicit density matrix propagation to elucidate the factors shaping Gd^{3+} DEER traces. The simulations show that mixing between the $|+\frac{1}{2}, -\frac{1}{2}\rangle$ and $|-\frac{1}{2}, +\frac{1}{2}\rangle$ states of the two spins, caused by the flip-flop term in the dipolar Hamiltonian, leads to dampening of the dipolar modulation. This effect may be mitigated by a large ZFS, or by pulse frequency settings allowing for a decreased contribution of the central transition and the one adjacent to it. The simulations reproduce both the experimental line shapes of the Fourier-transforms of the DEER time domain traces, and the trends in the behaviour of the modulation depth, thus enabling a more systematic design and analysis of Gd^{3+} DEER experiments.

I. INTRODUCTION

Gd^{3+}-based spin labels are an attractive alternative to nitroxide labels in Double Electron-Electron Resonance (DEER, also called Pulsed Electron-Electron Double Resonance, PELDOR) distance measurements, particularly at high fields, where they offer high sensitivity. Other advantages are the absence of orientation selection effects and chemical stability that makes them suitable for *in-cell* distance measurements. Gd^{3+}-Gd^{3+} DEER has been successfully used to measure intramolecular distance distributions in model compounds[1,2], proteins[3–6], nucleic acids[7,8], peptides in solution[9] and in model membranes[10,11], and nanoparticles.[12] Recently several *in-cell* Gd^{3+}-Gd^{3+} DEER experiments were demonstrated as well.[13–17] While most Gd^{3+}-Gd^{3+} distance measurements are carried out using DEER, it has recently been shown that Relaxation Induced Dipolar Modulation Enhancement (RIDME)[18] also works well for Gd^{3+}[19,20], and that high-field (240 GHz) continuous-wave EPR[21,22] can be used to extract distances from the width of the central transition. Gd^{3+}-nitroxide DEER measurements have also been reported.[23,12,24,25]

The DEER experiment measures the dipolar coupling frequency ω_{dd} between two spins, referred to as the "pump" and the "observer" spins, from which the distance can be extracted[26]. DEER pulse sequences generate a Hahn echo[27] or a refocused echo[28] at the observer spin frequency, and dipolar coupling is reintroduced using an inversion pulse at the pump spin frequency (Figure 1). Plotting the echo intensity against the time of the pump pulse insertion point produces a modulation of the echo intensity at the dipolar frequency. For a pair of spins with $S=\frac{1}{2}$, under the weak coupling approximation and in the absence of exchange interaction and spectral overlap between the pumped and observed spins[29], the echo intensity $V(t)$ in the DEER trace is given by[27]:

$$V(t) = V_0 \left\{ 1 - \lambda \left[1 + \int_0^{\pi/2} \cos(\omega_{dd}t)\sin\theta d\theta \right] \right\} \tag{1}$$

where V_0 is the echo amplitude in the absence of the pump pulse, λ is the modulation depth parameter representing the fraction of pumped spins excited by the pump pulse[26], θ is the angle between the inter-spin vector and the applied magnetic field, and the dipolar coupling frequency is

$$\omega_{dd} = \frac{\mu_0 g^2 \beta_e^2}{4\pi\hbar r^3}\left(3\cos^2\theta - 1\right) \tag{2}$$

2

where μ_0 is the vacuum permeability, g is the electron g-factor, β_e is the Bohr magneton, $\hbar$ is the reduced Planck's constant, and r is the inter-spin distance. In the absence of spin relaxation processes, DEER sensitivity is therefore given by λV_0. Many sophisticated methods exist for extracting the distance distribution from $V(t)$; they are implemented in the popular *Deer-Analysis* package[30,31] and elsewhere[32–34].
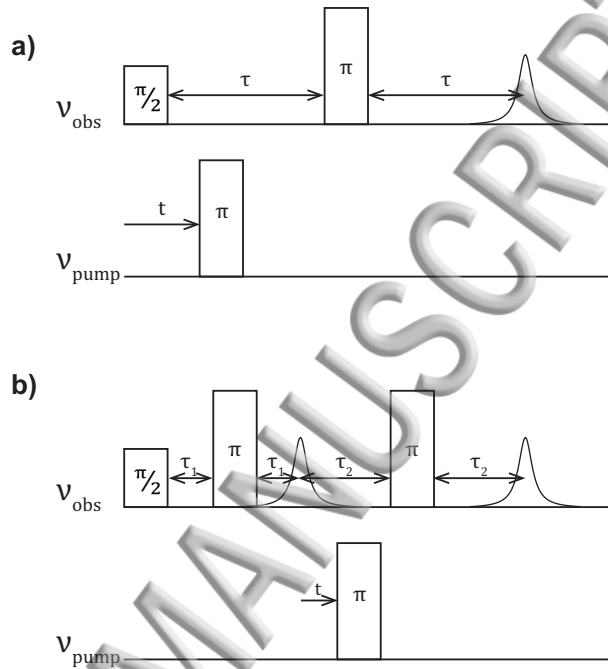
Figure 1: a) Three[27]- and b) four[28]-pulse DEER sequences. In both sequences, an echo is generated by pulses at the observer spin frequency ν_{obs}, and the application of the pump pulse at the ν_{pump} frequency causes a partial dephasing in that echo. The pump pulse time t is incremented to measure the dipolar frequency.

In previous work using Gd^{3+}-Gd^{3+} DEER, it was assumed (under the weak dipolar coupling approximation) that if the pump pulse flips Gd^{3+} by only a single quantum, then Gd^{+3}-Gd^{3+} DEER could be analysed as an effective $S=\frac{1}{2}$ system[1]. However, despite the practical success of those measurements, DEER traces obtained for model compounds with Gd^{+3}-Gd^{3+} distances below 4 nm displayed features not predicted by the theory for a $S=\frac{1}{2}$ pair under the weak dipolar coupling approximation[1,2,35]. Specifically, the dipolar spectrum (Fourier transform of the DEER traces) may deviate from the Pake pattern[1,2,36]. This deviation leads to a broadening of the distance distribution and the emergence of spurious distance peaks when the data is analysed by the software designed for spin-1/2 systems. This effect is larger for Gd^{3+} ions

with a smaller zero field splitting (ZFS) and a narrower central line[2,37]. Another unexpected feature is the low modulation depth[1,2]. These observations likely result from the different spectroscopic characteristics of Gd^{3+} compared to nitroxides – the high spin and the ZFS, which affect the validity of the weak dipolar coupling approximation.[2,35,36,38] An understanding of the factors shaping the DEER trace is therefore essential for the proper data analysis, and for the educated choice of optimal experimental parameters such as pulse frequencies and the chelate coordinating the Gd^{3+} ion.

The prior work on the subject has explored the limits of the effective S=1/2 and weak dipolar coupling approximation for Gd^{3+}-Gd^{3+} DEER using a simple frequency domain approach: transition energies were computed by diagonalizing the Hamiltonian, and were shown to shift due to the mixing between the $|+\frac{1}{2}, -\frac{1}{2}\rangle$ and $|-\frac{1}{2}, +\frac{1}{2}\rangle$ states by the flip-flop term of the dipolar interaction at short distances.[2,39] A large ZFS was found to reduce this mixing because it reduces the probability of overlap between the central transitions of the two spins in disordered samples with a large distribution over ZFS parameters, as commonly found for Gd^{3+} [40,41]. This understanding has led to proposals for experimental setups that can overcome the difficulties in the measurement of short distances[20,36,42]. However, this approach did not clarify the origin of the modulation depth problem, suggest optimal pulse settings in the DEER experiment, account for the possible rhombicity in the ZFS, or consider contributions from multiple transitions to the final DEER trace.

To address both the lineshape and the modulation depth, we carried out time-domain simulations of the DEER experiment using explicit density matrix propagation in *Spinach*[43]. Our goal was not fitting the DEER traces, but rather characterizing the effect of ZFS, dipolar state mixing, and pulse parameters on the DEER trace, including the modulation depth, damping rate, the shape of the Fourier transform, and the extracted distance distribution. The simulation considers all transitions between all energy levels at the specified temperature, the dipolar coupling including the flip-flop terms, the rhombic ZFS tensor up to the second spherical rank (and its ensemble distribution), as well as explicitly simulated soft microwave pulses.

We found that the simulation reproduces the experimental lineshapes, but overestimates the modulation depth. It confirms that the state mixing between the $|+\frac{1}{2}, -\frac{1}{2}\rangle$ and $|-\frac{1}{2}, +\frac{1}{2}\rangle$ states of the two spins, caused by the flip-flop terms in the dipolar Hamiltonian, leads to a strong damping of the dipolar modulation, and to artefacts in the distance distribution when software designed for spin 1/2 systems is used for the analysis.

II. THEORY

The spin Hamiltonian of two electrons with isotropic g-tensors and spin $S > \frac{1}{2}$, such as Gd^{3+} or Mn^{2+}, interacting via the dipolar mechanism and hyperfine coupled each to its own nucleus, is given by:

$$\hat{H} = \sum_{k=1,2} \left(\frac{g\beta_e B_0}{h} \hat{S}_{z,k} + \hat{S}_k \cdot \boldsymbol{D}_k \cdot \hat{S}_k + \hat{S}_k \cdot \boldsymbol{A}_k \cdot \hat{I}_k \right) + \hat{S}_1 \cdot \boldsymbol{T} \cdot \hat{S}_2 \tag{3}$$

Where the first term is the Zeeman interaction, the second is the zero-field splitting, the third is the hyperfine interaction with the corresponding nucleus (Gd has two magnetic isotopes with the total abundance of 30%[44]), and the fourth is the dipolar interaction between the two electrons.

The ZFS is adequately described by the usual D and E parameters:

$$D = \tfrac{3}{2} D_z, \quad E = \frac{D_x - D_y}{2} \tag{4}$$

accounting for its rank 2 part[45]. Higher-order terms (spherical ranks 4 and 6), although present for Gd^{3+}, are much smaller and can be neglected[46]. D_x, D_y, D_z are the principal values of the $\boldsymbol{D}$ tensor. In the eigenframe of the $\boldsymbol{D}$ tensor, the ZFS Hamiltonian is:

$$\hat{H}_{ZFS} = D\left(\hat{S}_z^2 - \frac{S(S+1)}{3} \right) + E\left(\hat{S}_x^2 - \hat{S}_y^2 \right) \tag{5}$$

The well-known second order perturbation analysis of the eigenvalues of this Hamiltonian[47,48] concludes that the energy of most transitions depends on D in the first order, whereas that of the central transition ($|-\frac{1}{2}\rangle \leftrightarrow |+\frac{1}{2}\rangle$) does so only in the second order. The central transition is therefore the narrowest, and gets narrower when the magnetic field is increased[47,48].

The dipolar coupling term in the spin Hamiltonian is given by[49]

$$\hat{H}_{dd} = \hat{S}_1 \cdot \boldsymbol{T} \cdot \hat{S}_2 = \frac{\omega_{dd}}{2\pi} \left[\hat{A} + \hat{B} + \hat{C} + \hat{D} + \hat{E} + \hat{F} \right] \tag{6}$$

where the secular term is

$$\hat{A} = \hat{S}_{z,1} \hat{S}_{z,2} \left(3\cos^2 \theta - 1 \right), \tag{7}$$

and the "flip-flop" (pseudo-secular) term is

5

$$\hat{B} = -\tfrac{1}{4}\left(\hat{S}_{+,1}\hat{S}_{-,2} + \hat{S}_{-,1}\hat{S}_{+,2}\right)\left(3\cos^2\theta - 1\right)$$

$$\text{(8)}$$

The terms $\hat{C}$, $\hat{D}$, $\hat{E}$, and $\hat{F}$ are negligible within the high field approximation, when the Larmor frequencies are much larger than the dipolar frequency, which is usually the case for common EPR spectroscopy. The flip-flop term $\hat{B}$ can usually be neglected (the "weak coupling" approximation) when the difference between the Larmor frequencies of the two electron spins is much larger than ω_{dd} ("unlike spins"). When this condition is not met ("like spins"), this term leads to state mixing. Powder averaging over all possible orientations in these two extreme cases yields a Pake pattern in the dipolar spectrum. For S=½, the singularities appear at ω_{dd} and $2\omega_{dd}$ for unlike spins, and at $3\omega_{dd}/2$ and $3\omega_{dd}$ for spins of identical Larmor frequencies. For intermediate regimes, the lineshape is more complicated[49,50].

Two isotopes of Gd are magnetically active, having a nuclear spin of 3/2: ^{155}Gd (natural abundance 14.8%, $\mu/\mu_N = -0.2582$) and ^{157}Gd (natural abundance 15.65%, $\mu/\mu_N = -0.3385$)[44]. The hyperfine coupling with these nuclei, ~14 MHz[51], is small and unresolved in the Gd^{3+} EPR spectrum. The effect of this hyperfine interaction on Gd^{3+}-Gd^{3+} DEER has not been explicitly addressed. However, Mn^{2+}-Mn^{2+} DEER measurements show that the effect of the dipolar flip-flop term is considerably smaller than in Gd^{3+}, which can be attributed to the inhibition of the dipolar state mixing by the hyperfine interaction[38,52] – the hyperfine coupling of ^{55}Mn (spin 5/2, 100% natural abundance), is much larger (~250 MHz).

III. METHODS

The implementation of the three-pulse (3P-) DEER sequence in *Spinach* considers the spin Hamiltonian in Equation (3) in its entirety except for the $\hat{C}$ through $\hat{F}$ terms of the dipolar interaction and the hyperfine interaction, which was found to have only a minor effect (Figure S1) and was therefore excluded from the calculations. The code performs explicit time domain propagation through off-resonance microwave pulses of finite power and width. It does not, however, include a background decay, relaxation, spectral diffusion, a distance distribution, instrumental factors such as B_1 inhomogeneity, or cross-excitation, *i.e.* the pump pulse exciting transitions of the observed spin and vice versa.

The spin system consists of two spin-7/2 electrons with identical isotropic *g*-values of 1.9925[53], because the Gd^{3+} *g*-anisotropy is unresolved at W-band[54]. Both spins have the same distributions of the ZFS parameters *D* and *E* (Figure 2)[40,41]: the *D* distribution is given by two Gaussians of identical width, centred around D_c and $-D_c$, whereas the *E/D* distribution is

given by $P\left(\frac{E}{D}\right) = \left(\frac{E}{D}\right) - 2\left(\frac{E}{D}\right)^2$. The ZFS values of two commonly used Gd^{3+} chelates, PyMTA[14] and DOTA[55], were used for the simulations. The ZFS distribution is integrated over to abolish orientation selection: every iteration of the loop picks D and E values at random and carries out the simulation, with the statistical weight assigned from the distribution. The ZFS values of the two spins are assumed to be identically distributed, but uncorrelated. D and E variation alone was found to be insufficient for abolishing orientation selection (data not shown), and therefore orientational freedom of the two ZFS tensors was also permitted. In accordance with the model underlying these distributions[40] and with experimental ENDOR results[56], a random ZFS orientation is picked for every iteration. The molecular frame was chosen to be that of the dipolar interaction, where the molecular Z axis coincides with that of the dipolar frame. Figure 3 shows the axis system used and the definitions of the various angles relating the ZFS of the two Gd^{3+} ions and their dipolar interaction. The ZFS distribution was sampled until convergence was observed, typically after ~150 samples (Figure S2), resulting in a computational time of about a week using 16 Xeon E5-2698 cores. The calculations were carried out either with the full dipolar Hamiltonian (labelled "$\hat{A} + \hat{B}$ dipolar") or just the secular term (labelled "$\hat{A}$ dipolar") to quantify the effect of the flip-flop term. Powder averaging was carried out using the rank 131 Lebedev grid[57,58].
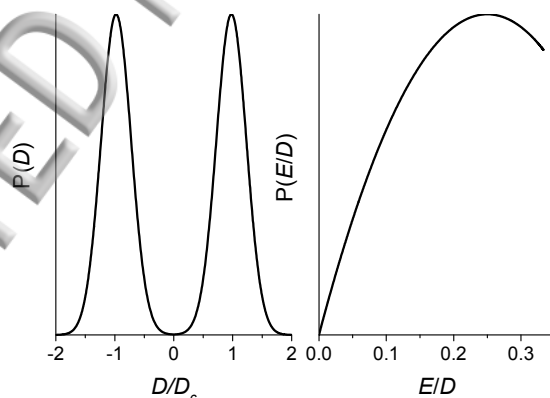
Figure 2: Representative distributions of ZFS parameters D and E used in the simulations. The D distribution is given by two Gaussians of identical width, centred around D_c and $-D_c$, whereas the E/D distribution is given by $\mathbf{P}\left(\frac{\mathbf{E}}{\mathbf{D}}\right) = \left(\frac{\mathbf{E}}{\mathbf{D}}\right) - \mathbf{2}\left(\frac{\mathbf{E}}{\mathbf{D}}\right)^2$. [40,41] Here D_c=1150 MHz, σ=300 MHz^2 (standard deviation, related to the full width at half maximum by $\mathbf{FWHM} = \mathbf{2}\sqrt{\mathbf{ln4}}\boldsymbol{\sigma}$), as in the commonly used Gd^{3+} chelate, PyMTA[14].
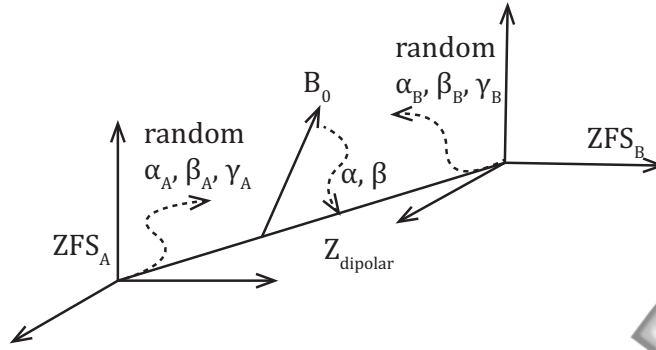
Figure 3: An illustration of the various axes frames used in the simulations and their relations, through the appropriate Euler angels, with respect to the Z axis of the dipolar interaction, $Z_{dipolar}$. The two ZFS frames have random orientations, sampled from the distribution shown in Figure 2 until convergence in the simulation results. Two-angle powder averaging is used with respect to the overall system orientation. The A spin is the observed spin and the B spin is the pumped spin.

The thermal equilibrium density matrix (used as the initial condition) was calculated at each orientation using the Boltzmann law:

$$\hat{\rho}_{eq} = \frac{\exp\left(-\hat{H}/kT\right)}{\mathrm{Tr}\left[\exp\left(-\hat{H}/kT\right)\right]} \tag{9}$$

The magnetic field was 3.5 T and the temperature was 10 K unless otherwise stated.

The three-pulse DEER experiment (Figure 1) was used in the simulation. The frequencies measured in the three- and four-pulse DEER variants are known to be the same for $S=\frac{1}{2}$[59], the difference being a higher echo intensity[59] and a slightly broader excitation profile[28] for the three-pulse variant, at the cost of having to deal with a dead time. For a high spin, the difference between the two techniques is unexplored.

In order to preserve all non-secular interactions, the simulations were carried out in the laboratory frame. The excitation was implemented by using either "ideal" pulses, for which the internal Hamiltonian was neglected during the pulse, or "soft" pulses, for which this approximation was not made. Transition-selective pulse operators were generated by constructing an $\hat{S}_x$ operator where only the matrix elements corresponding to the desired transition were nonzero, and constructing the pulse propagator to be $e^{-i\frac{\pi}{2}\hat{S}_x}$ or $e^{-i\pi\hat{S}_x}$ to represent a $\pi/2$ or π pulse, respectively. Such pulses excite or invert a given transition perfectly – an oversimplification used to compare the behaviour of different transitions. The

simulation of the more realistic soft off-resonance pulses was carried out by including the internal Hamiltonian into the pulse propagator, computing the time-ordered propagator over the pulse waveform period and taking a matrix logarithm to obtain the effective Hamiltonian[60,61]. This Hamiltonian was then applied for the duration of the pulse. The reason why matrix logarithm is used to obtain the generator (instead of just multiplying the period propagator up to the desired pulse duration) has to do with numerical efficiency – propagator multiplication method is expensive when the time interval ratio is not a power of 2. The B_1 value needed for the desired pulse durations was found by simulating a nutation experiment (Figure S3).

Gd^{3+} spin echoes under the ideal pulse conditions are narrow and easy to miss. They also shift in a hard to predict way when soft pulses are used. A 2D detection was therefore employed in the simulation – a 600 ns interval centered around the expected echo position was computed for each pump pulse location point. For soft pulse simulations, the echo was integrated over an integration window of the echo full width at half height (Figure 4); for ideal pulse simulations, its maximum value was used.

Theoretical DEER traces were post-processed in the following way: (1) normalized to the maximum, (2) passed though a Savitzky-Golay filter to eliminate minor high frequency wobbles resulting from non-random pulse phases in the simulation, as well as imperfect powder and ZFS distribution averaging, (3) vertically shifted to oscillate around zero by subtracting the mean of the second half of the trace, (4) apodized using the Hamming window function, (5) zero-filled to three times their original length, and (6) Fourier transformed. Distance distributions in the spin-1/2 approximation were obtained using Tikhonov regularization in *DeerAnalysis*[31] (see Figure S4 in the SI). The fits to the time and frequency signals according the distance distributions were good for long distances, but not for short ones, due to the dead-time of the 3P-DEER experiment (Figures S4 and S9 in the SI).
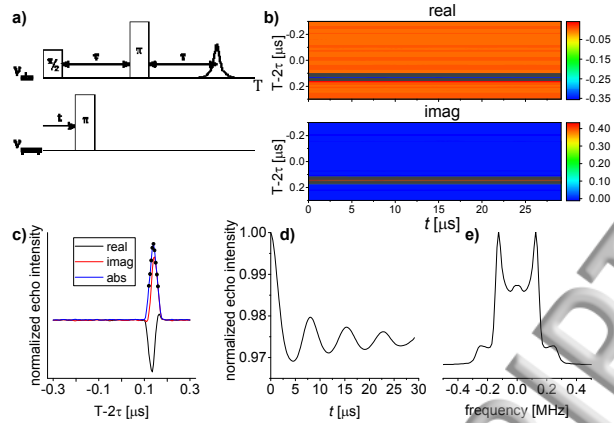
Figure 4: A schematic of the 2D DEER detection described in the main text. a) The pulse sequence, showing the pump pulse timing t and the transient trace coordinate T. b) Echo intensity along the acquisition time T versus pump pulse timing t. c) Echo intensity along the acquisition time at pump pulse timing t=0, showing the time points used for echo integration. d) DEER trace obtained by integrating the echo intensity and applying Savitzky-Golay filtration and e) its FT. The dataset used is r=7.2 nm, D=1150±300 MHz, observer pulses of 15/30 ns on the centre and pump pulse of 15 ns 100 MHz higher.

IV. RESULTS AND DISCUSSION

A. Echo-detected EPR spectra

Two commonly used Gd^{3+} chelates, PyMTA[14] and DOTA[55], were chosen for the simulations. Their experimental echo-detectd EPR (ED-EPR) spectra are shown in Figure 5, along with *EasySpin*[62] simulations to confirm the ZFS values and their distributions, which were then used for the DEER simulations.
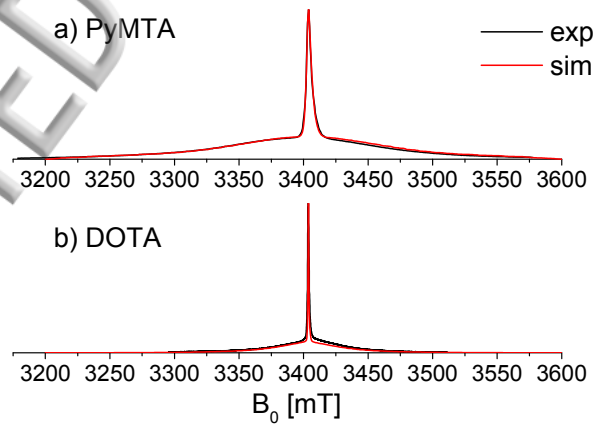

Figure 5: *EasySpin*[62] simulations of the W-band ED-EPR spectra of the Gd^{3+} chelates studied in this work: a) PyMTA[2], D=1150±300 MHz, linewidth=1.5 MHz; b) DOTA[36], D=500±190 MHz, linewidth=0.5 MHz.

B. Ideal pulse DEER simulations

Initially we simulate Gd^{3+}-Gd^{3+} DEER using ideal transition-selective pulses. These pulses perform a perfect population inversion along selected transitions. This allows characterizing

the behaviour of various transitions. Such DEER traces were simulated for a short (2 nm) and a medium (5 nm) distance for two different ZFS distributions. The results (Figure 6) show that for the $\hat{A}$ dipolar case (black traces), all DEER traces produce perfect Pake patterns. As expected, the modulation is deeper for lower m_s values of the pumped transition, due to the thermal polarization, and it does not depend on the ZFS (which of course only holds true for ideal pulses, whose excitation efficiency is independent of the EPR spectral linewidth) or distance.

For the $\hat{A} + \hat{B}$ dipolar coupling case (red traces), the modulation is damped. The damping is manifested in the frequency domain as a smearing of the Pake pattern singularities. This is more pronounced at short distances. In the setups where the central transition is observed and either the $|-\frac{7}{2}\rangle \leftrightarrow |-\frac{5}{2}\rangle$ or the $|-\frac{5}{2}\rangle \leftrightarrow |-\frac{3}{2}\rangle$ transition of spin B is pumped, the spectra still maintain the general form of a Pake pattern. However, in the setup where the central ($|-\frac{1}{2}\rangle \leftrightarrow |\frac{1}{2}\rangle$) transition of spin A is observed and the adjacent ($|-\frac{3}{2}\rangle \leftrightarrow |-\frac{1}{2}\rangle$) of the B spin is pumped, or vice versa, the modulation in the time domain is nearly lost, as is the Pake pattern. Also unique to these setups is the fact that the dipolar flip-flop process (the $\hat{B}$ term) slightly decreases the modulation depth for the short distance. A long distance moderates the damping, especially together with a large ZFS, and also prevents the reduction of modulation depth. This is in accordance with experimental results, showing that the distortions in the DEER spectra are more severe for short distances[2] and for chelates with a small ZFS[2,36], and are alleviated by pulse setups decreasing the contribution of the $|-\frac{3}{2}\rangle \leftrightarrow |-\frac{1}{2}\rangle$ transition[36]. When switching between the pumped and observed transitions, the behaviour is analogous (see Figure S5).

11
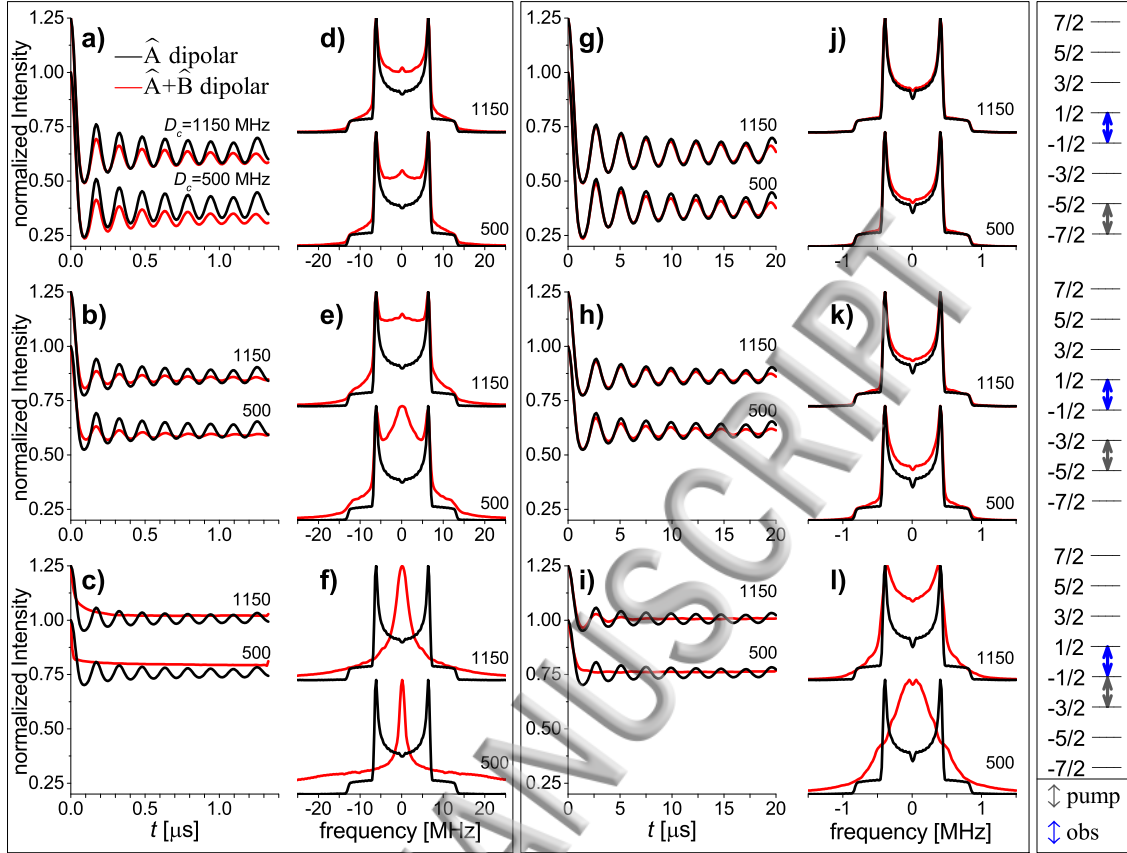
Figure 6: Simulated DEER traces and spectra using ideal transition-selective pulses. The observer pulses were set to excite the central transition, and the pump pulse was set to the |-7/2>↔|-5/2> (top row), |-5/2>↔|-3/2> (second row), or |-3/2>↔|-1/2> (third row) transitions. The energy level diagrams show the pump (grey) and observer (blue) pulses setup for the corresponding rows. r=2.0 nm (a-f) or 5.0 nm (g-l), D=500±190 or 1150±300 MHz, vertically shifted for clarity. The dipolar Hamiltonian consisted of either both the $\hat{A} + \hat{\boldsymbol{B}}$ terms (red lines) or the $\hat{A}$ term (black lines).

The modulation dampening is expected based on previous calculations[2,39] which attributed it to state mixing between the |+½, –½> and |–½, +½> states by the dipolar flip-flop term. This mixing is present because the only energy difference between these two states is caused by the second order contribution of the ZFS[47,48], which is quite small. Therefore, the weak coupling approximation fails: the off-diagonal flip-flop term is not negligible with respect to the difference between the energy levels it connects, and it can efficiently mix them. This mixing changes the energy of the observer transitions involving these states, particularly $|-\frac{3}{2},\frac{1}{2}>$ ↔ $|-\frac{1}{2},\frac{1}{2}>$ excited here, so that the eight lines in the multiplet of a given observer transition are no longer equally spaced by the dipolar frequency[39]. Since it is the spacing between these lines which is measured in DEER, when a transition involving a mixed state is excited, the measured frequency will not be the nominal dipolar frequency ω_{dd}, but another value, depending on the ZFS and the particular transition and manifold involved. As the ZFS is anisotropic and

12

displays a broad distribution, and several transitions are simultaneously excited, many different frequencies will be measured. These frequencies interfere with each other, damping the modulation even in the absence of a distance distribution. A similar behaviour was described for Mn^{2+}-Mn^{2+} DEER[38]. It is noteworthy that the slight smearing of the dipolar spectrum in the other setups indicates a residual effect of dipolar mixing, even for the large $|m_s|$ values. The change in modulation depth due to the $\hat{B}$ term probably results from changes in the transition probability following state mixing.

Since the distortions are significant only when the excited transitions are $|-\frac{3}{2}\rangle \leftrightarrow |-\frac{1}{2}\rangle$ and $|-\frac{1}{2}\rangle \leftrightarrow |+\frac{1}{2}\rangle$, it may be hypothesized that the cause is the adjacency of the excited transitions. However, that is not actually the case: when another pair of adjacent transitions are excited, these strong distortions are absent (Figure S6 in the SI), confirming that this behaviour is unique to the narrow central transition. Nonetheless, one can still observe a smaller effect of the state mixing by the flip-flop term in nearly all pulse setups, particularly at short distances.

Even these results, obtained using the oversimplified approach of transition-selective pulses, can show that as suspected, dipolar state mixing is the cause of the artificial broadening of the distance distribution in Gd^{3+} DEER, and can reproduce the experimentally observed ability of a long distance or a large ZFS to moderate this. These results also indicate that not all transitions behave the same; the question of how affected the DEER trace becomes, is therefore the question of which transitions are involved.

C. Soft pulse DEER simulations

To study the effect of the simultaneous excitation of several transitions, we turned to simulating Gd^{3+}-Gd^{3+} DEER using soft pulses. Such simulations allow for a more direct comparison with the experimental data obtained using rigid model compounds, which serves both to test the simulation validity and to account for experimental observations.

1. Pulse configuration

We have established above (Figure 6) that not all transitions behave the same under dipolar state mixing. This naturally leads to the question of whether an application of pulses, maximizing the contribution of the lower lying transitions ($|-7/2\rangle \leftrightarrow |-5/2\rangle$, $|-5/2\rangle \leftrightarrow |-3/2\rangle$) at the expense of the $|-3/2\rangle \leftrightarrow |-1/2\rangle$ one, allows overcoming the problems of Gd^{3+} DEER.

A previous work[36] showed that a large frequency separation $\Delta\nu$ between the excitation frequencies mitigates the deviations from the Pake pattern. A series of DEER traces using

different Δv values and their simulations are shown in Figure 7. The time domain traces and the modulation depth values are shown in Figure S7, S8 respectively, in the SI. The simulations reproduce the gradual recovery of the modulations and the Pake pattern with an increasing Δv, together with the moderation of the distance distribution broadening. These effects are confirmed to result from dipolar state mixing, and their gradual reduction can be explained by an increase in the contribution of the $|-5/2>\leftrightarrow|-3/2>$ and $|-7/2>\leftrightarrow|-5/2>$ transitions to the signal at the expense of the $|-3/2>\leftrightarrow|-1/2>$ transition as Δv increases. These simulations are also in line with RIDME results, which show that broadening due to the dipolar flip-flop term is significanly reduced as in this experiment the contributions of the $|-7/2>\leftrightarrow|-5/2>$, $|-5/2>\leftrightarrow|-3/2>$ transitions are substantial[20]. It must be stated that Gd^{3+}-RIDME, despite its ability to moderate the problems of Gd^{3+}-DEER, suffers from a problem of its own – the contribution of higher harmonics to the signal, whose manifestation in the distance distribution may be hard to distinguish from additional distances[19,20]. A comparison between excitation schemes where the pump pulse is set to the powder pattern center or off-center is shown in Figure S9. A spectral distortion is noticeable even in the absence of dipolar mixing. This is caused by the inherent dead-time problem of the 3P-DEER sequence (see Figure S10, SI).

The simulation reproduces the experimental lineshape to a reasonable degree; considering some uncertainty in the ZFS distribution, the effect of experimental background subtraction, and the experimental distance distribution, a perfect reproduction of the experimental data cannot reasonably be expected.
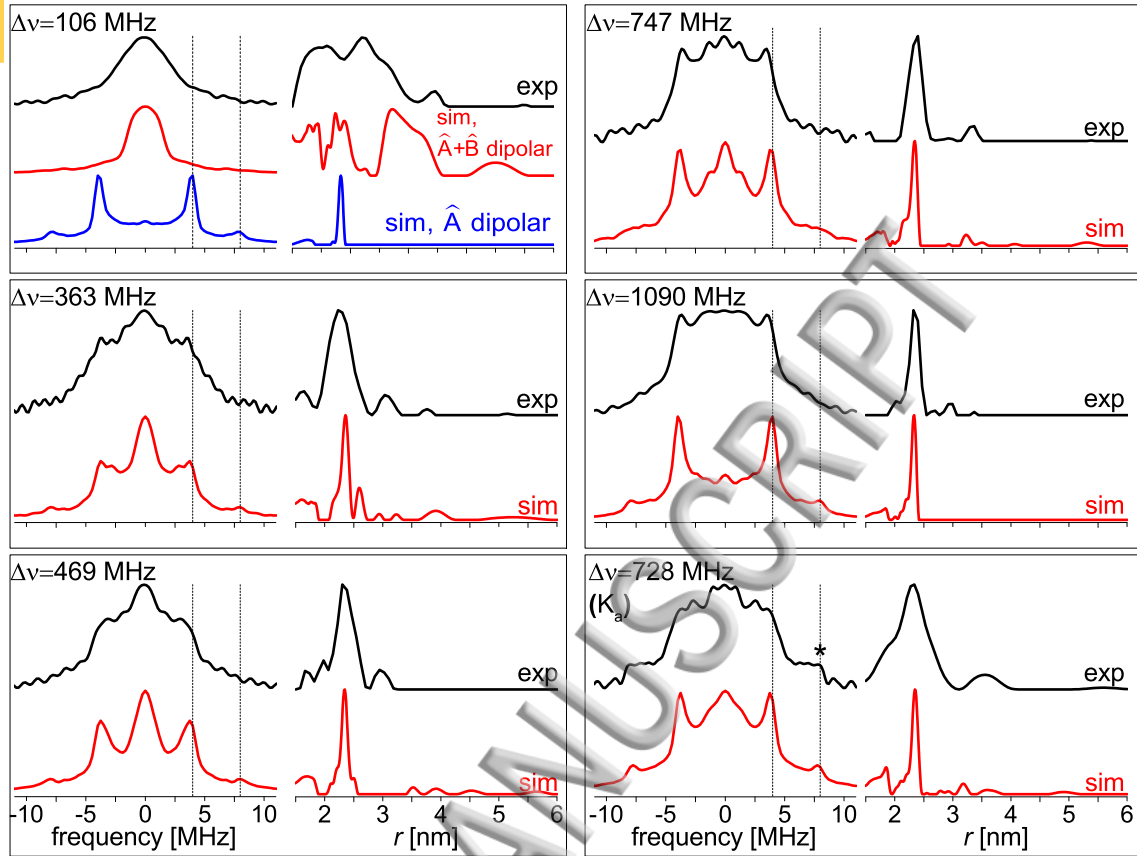
Figure 7: Comparison between simulated and experimental DEER spectra and distance distributions (obtained using *DeerAnalysis*[31]) for various pulse frequency separations $\Delta\nu$. For the setup with $\Delta\nu$=106 MHz, the spectrum and distance distribution for the $\hat{A}$ dipolar coupling case are shown as a representative example. The dashed lines indicate the expected positions of the Pake pattern singularities. The asterisk in the Ka band spectrum shows the position of the ^{2}H modulations present in the experimental spectrum. Pulse setup: pump pulse on the centre, pulse durations shown on Table I. r=2.35 nm, D=500$\pm$190 MHz. Experimental data taken from[36]. The time domain data is in Figure S7 in the SI.

Table I: Pulse durations for DEER using various pulse frequency separations $\Delta\nu$ shown in Figure 7.

$\Delta\nu$ [MHz]	106	363	469	747	1090	728 (Ka band, T=15 K)
obs [ns]	15,30	17.5, 35	17.5, 35	20,40	17.5, 35	6,12
pump [ns]	25	30	25	35	25	10

2. Effect of the Distance

Experimentally, it was observed that the characteristic problems of Gd^{3+}-DEER are moderated by a long distance[2]. To check if the simulation reproduces this behaviour, Figure 8 shows a comparison between simulated and experimental[2] DEER traces and spectra of

PyMTA-based rulers, for a short (1.95 nm) and a medium (4.75 nm) distance. The short distance was also measured in Q-band, in addition to W-band.
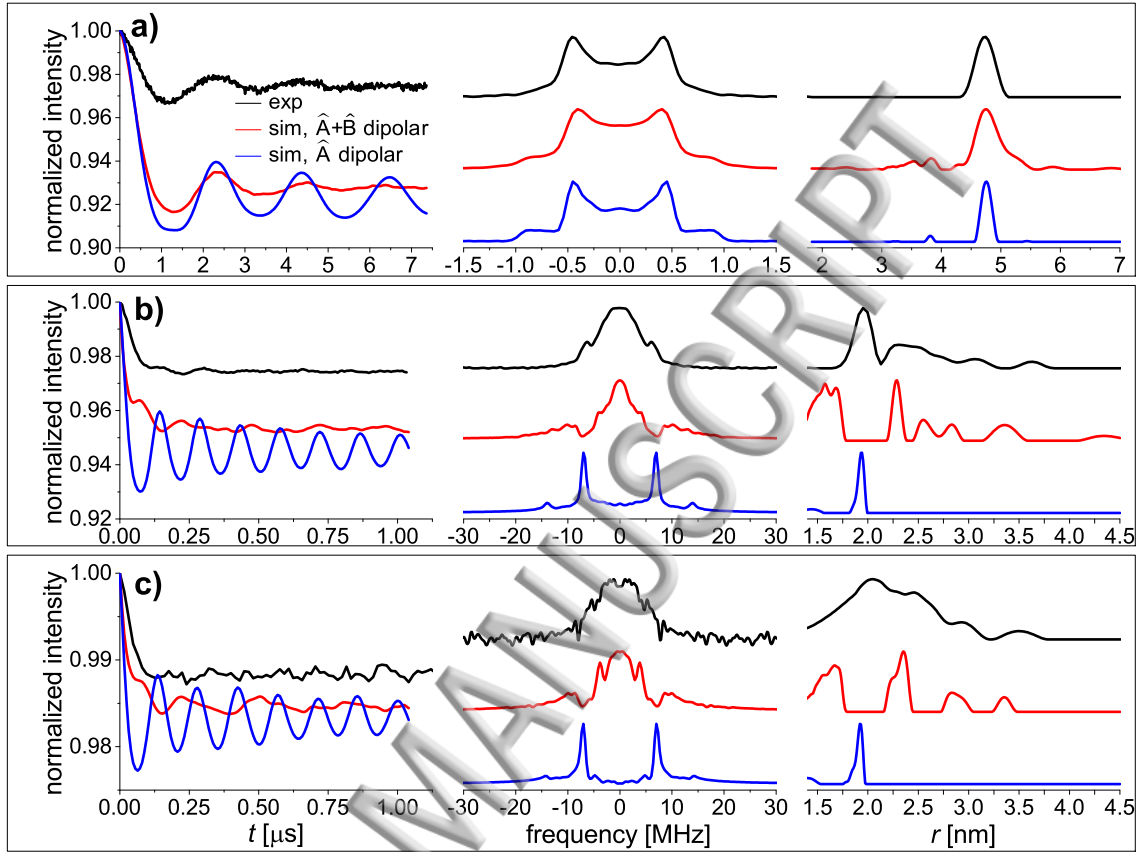
Figure 8: Comparison between simulated and experimental DEER traces for a) a medium (4.75 nm) and b,c) a short (1.95 nm) distance. (a) and (b) were simulated for W-band, (c) for Q-band. First column: time domain traces. Second column: DEER spectra. Third column: distance distributions obtained using the spin-1/2 approximation. W-band setup: pump pulse on the centre, t_{pump}=15 ns, $\Delta\nu$=90 MHz, $t_{\pi/2}$=15 ns. Q-band setup: pump pulse on the centre, t_{pump}=28 ns, $\Delta\nu$=100 MHz, $t_{\pi/2}$=20 ns. D=1150$\pm$300 MHz. Experimental data taken from[2].

At W-band, the calculated modulation depth is overestimated by a factor of about 2-3 compared to the experimental one. At Q-band, the overestimation is less pronounced. The dipolar flip-flop term slightly decreases the modulation depth, more so for the short distance. A comparison between the results with (red lines) and without (blue lines) dipolar flip-flop terms shows that dipolar mixing considerably dampens the modulation, nearly abolishing it for the short distance, where the associated spectrum strongly deviates from a Pake pattern and spurious peaks appear in the distance distribution. This is a consequence of the use of a distance distribution analysis kernel designed for the weak-coupling case, which interprets the many frequency components in the DEER trace as representing different distances. These

16

results confirm that the weak-coupling approximation does indeed fail in Gd^{3+} DEER at short distances. The use of the weakly coupled spin-1/2 assumption during the distance distribution extraction for short distances and small D values leads to a nonsensical answer. Software packages must therefore be extended to the full spin-7/2 case before they can be used in this context. However, this may be impractical because of the excessive computational time and the need for an exact knowledge of the ZFS parameters and their distributions, which is not always available. A more practical way would be the use of chelates with a large ZFS or of different experimental conditions[20,36].

The modulation depth decreases for short distances (<2.9 nm), independently of dipolar mixing (see Figure S11), which may be due to the central line broadening by the dipolar interaction[35]. For longer distances, the modulation depth is independent of the distance. Dipolar mixing only slightly decreases the modulation depth. The simulated modulation depth values are about twice as large as the experimental ones.

3. ZFS vs distance

The ultimate goal of the simulation is to enable an educated choice of experimental parameters. An important question is which tag (or which ZFS value) is the most suitable for which distance. It has been suggested[2] that tags with a large ZFS are more suitable for short distances, because the large ZFS reduces the distortions due to the dipolar flip-flop terms, whereas those with a small ZFS are suitable for long distances, where dipolar mixing poses less of a problem, and the narrow central line offers improved sensitivity. To validate this, a set of DEER traces using different distances and ZFS values was simulated.

The results (Figure 9) show that for r = 2.2 or 3 nm, no ZFS in the range of 500-2000 MHz could overcome the dipolar mixing. Most spin-1/2 model reconstructions do not even predict the right distance (those that do, may do so by a coincidence, because that happens for the smaller ZFS). Only for r = 4 nm does the real distance appear, being slightly shifted up for D_c < 950 MHz. Even then, there is a substantial broadening, and a ghost peak that may be the second harmonic of the dipolar frequency. The simulations are, however, more pessimistic than the reality: experimentally, even for $r \sim 2$ nm, the real distance can be extracted[2].

It is noteworthy that, in the absence of the dipolar mixing, the shape of the Fourier transform of the DEER trace is independent of ZFS (Figure S12 in the SI). This indicates that the slight tilting of the electron spin quantization axis by the ZFS has practically no effect in DEER at W-band, in agreement with what was found before[1,35,63,39], even in Q-band[1,12].
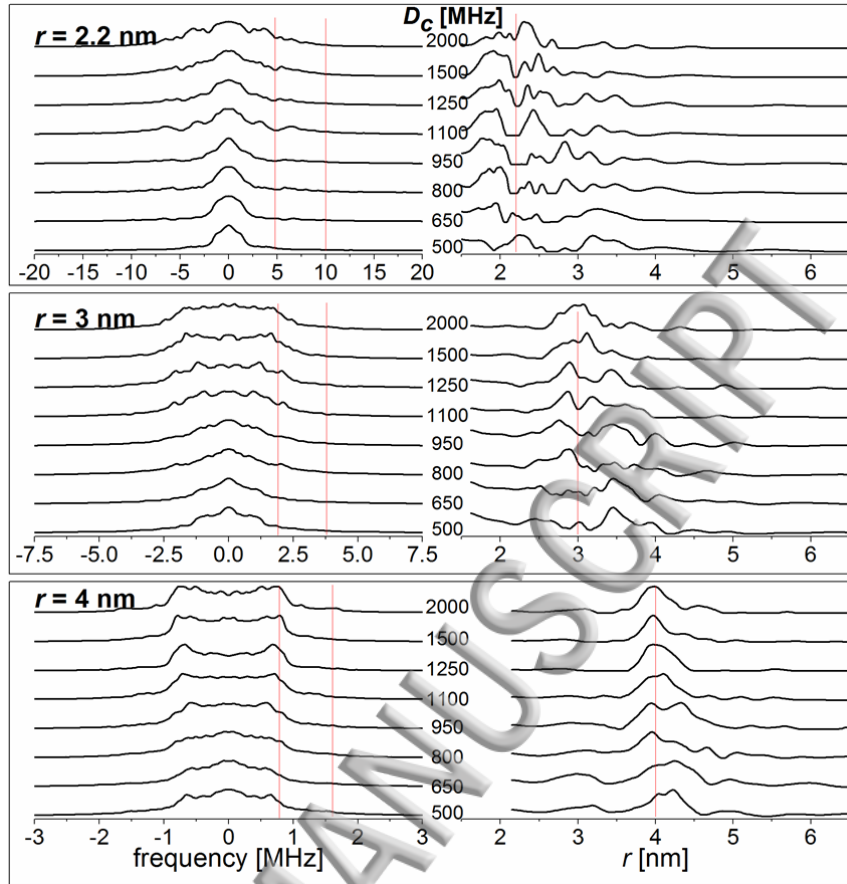
Figure 9: Dipolar spectra from simulated DEER traces and corresponding distance distributions obtained using *DeerAnalysis* for various distances and ZFS values. Pulse setup: pump pulse on the centre, t_{pump}=15 ns, $\Delta\nu$=100 MHz, $t_{\pi/2}$=15 ns. The standard deviation of the D Gaussian distribution was arbitrarily chosen to be always half the size of the average D. The horizontal lines show the expected positions of the singularities of the Pake patterns and the distances.
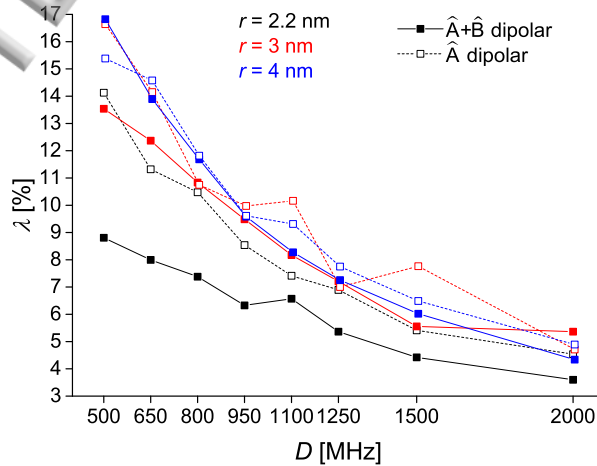
Figure 10: Modulation depth values for the simulated DEER traces shown in Figure 9.

The modulation depth decreases with the ZFS, as expected due to broadening of the central transition that is pumped here. It also decreases for short distances, even without the dipolar mixing, due to the broadening of the central transition by the dipolar coupling. Dipolar mixing decreases the modulation depth for the shortest distance only. The width of the distribution of D also affects both the modulation depth and the spectral lineshape (Figure S13 in the SI).

D. Additional factors

The simulation predicts a more severe effect of dipolar mixing on the distance distribution than that experimentally observed (Figure 8, Figure 9), and systematically overestimates the modulation depth. One possible factor which can affect DEER traces and was not considered is cross-excitation, that is, the ability of each excitation frequency to excite not only the spin it is intended for, but also the other spin, which is of course inevitable in practice. As the excitation of both spins by both frequencies results in no modulation, such cross-excitation may exclude some of the strongly coupled spin pairs, which are affected the most by the dipolar pseudosecular term, from the DEER trace.

It is known that the application of the pump pulse causes a decrease of the echo intensity, probably by the formation of undetectable multiple-quantum coherences due to an effect of the pump pulse on transitions of the observed spin[12,64,65]. This echo reduction effect increases with the modulation depth[65], and therefore the optimum modulation depth value is not the largest achievable one. This effect is not studied in the current work, where cross-excitation is not included.

Another possible factor suspected to decrease the experimental modulation depth is random flips of the pumped spin owing to spectral diffusion. An odd number of such flips cancels out the effect of the pump pulse, and therefore decreases the modulation depth. Spectral diffusion can be mediated by spin diffusion – flips with neighboring spins which are not excited in the experiment, caused by the pseudosecular part of the dipolar interaction. As spin diffusion is more effective when the frequencies of the two spins are similar[35], its effect on the modulation depth is expected to be stronger when the narrow central transition is pumped, and also to be more pronounced in higher field, because the central line narrows with the high field[47,48]. Experimental results show the depth to decrease with the evolution time[9,65], which can be explained by the longer evolution time allowing more time for random flips to occur. As the simulation considers only one spin pair participating in DEER, this effect is not

19

accounted for. The simulation shows no effect of the evolution time on the modulation depth (data not shown).

Other factors missing from the simulation are the lack of phase coherence between the different pulses of the DEER experiment on our hardware (this should have no effect for the spin-selective pulses used here), B_1 inhomogeneity, and uncertainty introduced by the background subtraction.

Finally, in this work we did not consider the distribution in the distance, which is always present in biomolecules and originates from some intrinsic flexibility of the biomolecule combined with the flexibility of the Gd^{3+} linker to the molecule. This additional broadening would mask some of the effects of the pseudosecular term on the extracted distance distribution.

V. CONCLUSIONS

We have presented a numerical simulation of time domain Gd^{3+}-Gd^{3+} DEER, considering the spin Hamiltonian in its entirety and accounting for soft pulses. The simulation confirms that state mixing between the $+\frac{1}{2}$ and $-\frac{1}{2}$ states of the two spins, caused by the pseudosecular term in the dipolar Hamiltonian, leads to damping of the dipolar modulation, and for a short distance also to a decrease of the modulation depth. The software designed for distance distribution extraction from spin-1/2 DEER data cannot therefore be used in good faith to process Gd^{3+} DEER traces for short distances and a small ZFS; a more sophisticated deconvolution kernel accounting for all the various processes described above is necessary to make that possible. However, an informed selection of experimental parameters, minimizing the effects of dipolar state mixing, is a more practical approach. Specifically, whenever a broad distance distribution is detected in the region below 4 nm, a RIDME measurement or a measurement with a large $\Delta\nu$ should be carried out to differentiate a genuinely broad distance distribution from an artificial broadening due to the pseudosecular terms of the dipolar interaction.

SUPPLEMENTARY MATERIAL

See supplementary material for additional information regarding the methodology (demonstration of convergence of the DEER trace upon integration over the ZFS, a nutation experiment simulation, example of extraction of the distance distribution) and results (the effect of the Gd^{3+} hyperfine interaction, simulations using ideal pulses, effect of pumping on-

vs off-center, dead-time dependent spectral distortions, modulation depth vs distance, the effect of ZFS vs that of the distance, and the effect of the width of the ZFS distribution).

ACKNOWLEDGMENTS
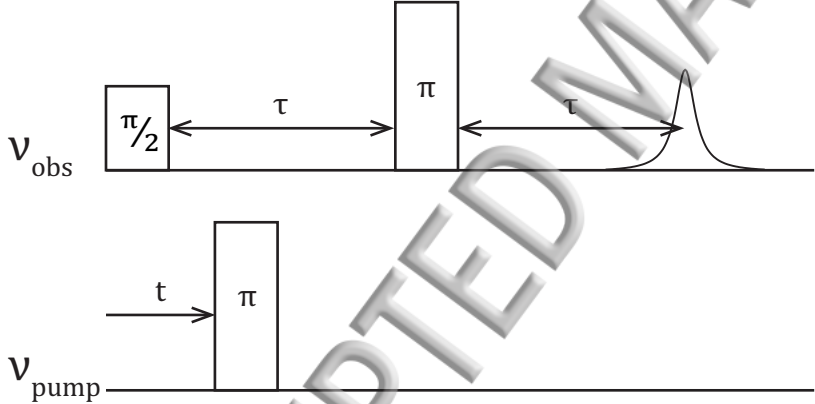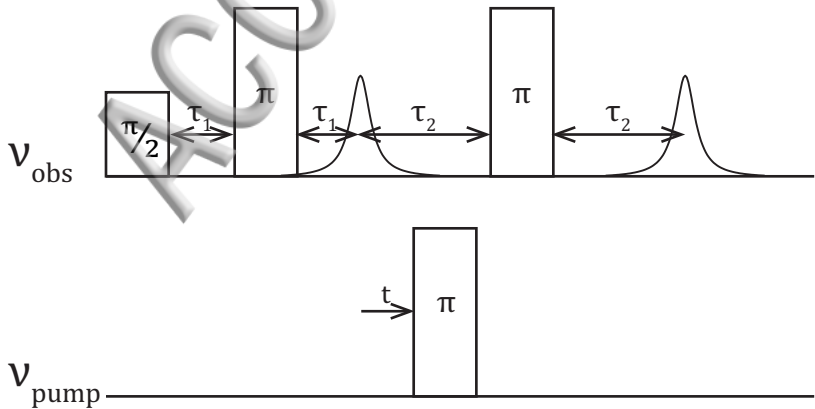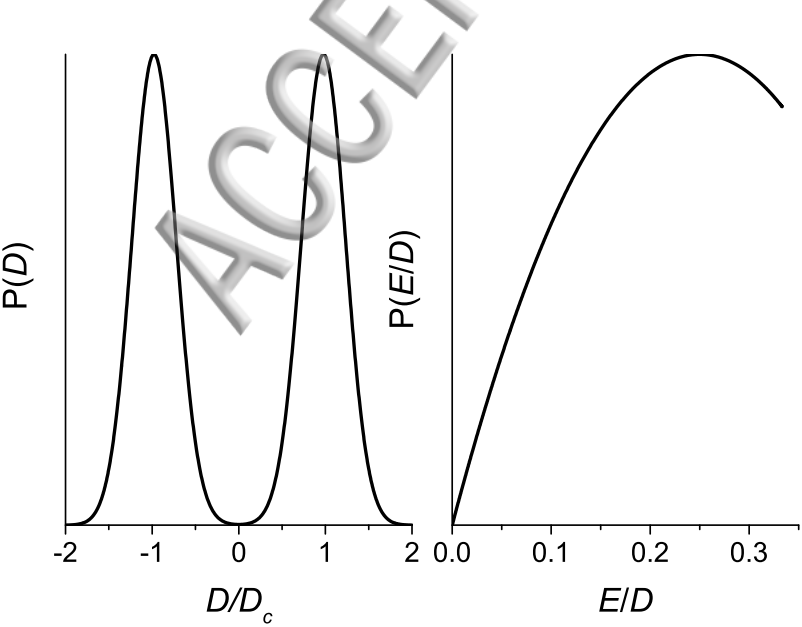
REFERENCES

[1] A.M. Raitsimring, C. Gunanathan, A. Potapov, I. Efremenko, J.M. Martin, D. Milstein, and D. Goldfarb, J. Am. Chem. Soc. **129**, 14138 (2007).

[2] A. Dalaloyan, M. Qi, S. Ruthstein, S. Vega, A. Godt, A. Feintuch, and D. Goldfarb, Phys. Chem. Chem. Phys. **17**, 18464 (2015).

[3] A. Potapov, H. Yagi, T. Huber, S. Jergic, N.E. Dixon, G. Otting, and D. Goldfarb, J. Am. Chem. Soc. **132**, 9040 (2010).

[4] H. Yagi, D. Banerjee, B. Graham, T. Huber, D. Goldfarb, and G. Otting, J. Am. Chem. Soc. **133**, 10418 (2011).

[5] D.T. Edwards, T. Huber, S. Hussain, K.M. Stone, M. Kinnebrew, I. Kaminker, E. Matalon, M.S. Sherwin, D. Goldfarb, and S. Han, Structure **22**, 1677 (2014).

[6] D. Barthelmes, M. Gränz, K. Barthelmes, K.N. Allen, B. Imperiali, T. Prisner, and H. Schwalbe, J. Biomol. NMR **63**, 275 (2015).

[7] Y. Song, T. Meade, A. Astashkin, E. Klein, J. Enemark, and A. Raitsimring, J. Magn. Reson. **210**, 59 (2011).

[8] F. Wojciechowski, A. Groß, I.T. Holder, L. Knörr, M. Drescher, and J.S. Hartig, Chem. Commun. **51**, 13850 (2015).

[9] M. Gordon-Grossman, I. Kaminker, Y. Gofman, Y. Shai, and D. Goldfarb, Phys. Chem. Chem. Phys. **13**, 10771 (2011).

[10] E. Matalon, T. Huber, G. Hagelueken, B. Graham, V. Frydman, A. Feintuch, G. Otting, and D. Goldfarb, Angew. Chem. **125**, 12047 (2013).

[11] N. Manukovsky, V. Frydman, and D. Goldfarb, J. Phys. Chem. B **119**, 13732 (2015).

[12] M. Yulikov, P. Lueders, M.F. Warsi, V. Chechik, and G. Jeschke, Phys. Chem. Chem. Phys. (2012).

[13] A. Martorana, G. Bellapadrona, A. Feintuch, E. Di Gregorio, S. Aime, and D. Goldfarb, J. Am. Chem. Soc. **136**, 13458 (2014).

[14] M. Qi, A. Groß, G. Jeschke, A. Godt, and M. Drescher, J. Am. Chem. Soc. **136**, 15366 (2014).

[15] F.C. Mascali, H. Ching, R.M. Rasia, S. Un, and L.C. Tabares, Angew. Chem. **128**, 11207 (2016).

[16] F.X. Theillet, A. Binolfi, B. Bekei, A. Martorana, H.M. Rose, M. Stuiver, S. Verzini, D. Lorenz, M. van Rossum, and D. Goldfarb, Nature (2016).

[17] Y. Yang, F. Yang, Y. Gong, J. Chen, D. Goldfarb, and X. Su, Angew. Chem. **129**, 2960 (2017).

[18] L. Kulik, S. Dzuba, I. Grigoryev, and Y.D. Tsvetkov, Chem. Phys. Lett. **343**, 315 (2001).

[19] S. Razzaghi, M. Qi, A.I. Nalepa, A. Godt, G. Jeschke, A. Savitsky, and M. Yulikov, J. Phys. Chem. Lett. **5**, 3970 (2014).

[20] A. Collauto, V. Frydman, M.D. Lee, E.H. Abdelkader, A. Feintuch, J.D. Swarbrick, B. Graham, G. Otting, and D. Goldfarb, Phys. Chem. Chem. Phys. **18**, 19037 (2016).
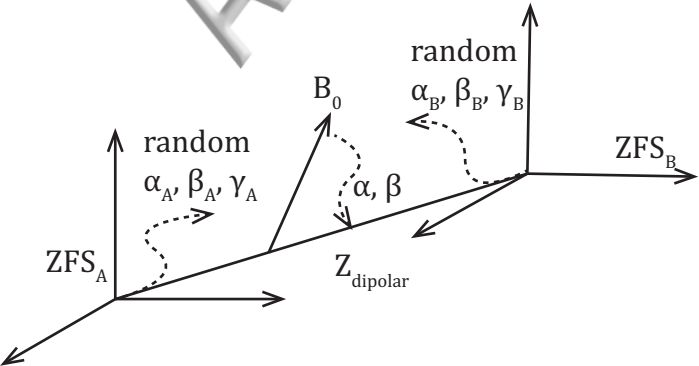
21 D.T. Edwards, Z. Ma, T. Meade, D. Goldfarb, S. Han, and M. Sherwin, Phys. Chem. Chem. Phys. (2013).

22 J.A. Clayton, M. Qi, A. Godt, D. Goldfarb, S. Han, and M. Sherwin, Phys. Chem. Chem. Phys. (2017).

23 P. Lueders, G. Jeschke, and M. Yulikov, J. Phys. Chem. Lett. **2**, 604 (2011).

24 I. Kaminker, I. Tkach, N. Manukovsky, T. Huber, H. Yagi, G. Otting, M. Bennati, and D. Goldfarb, J. Magn. Reson. **227**, 66 (2013).

25 M. Yulikov, in *Electron Paramagn. Reson.* (Royal Society of Chemistry, 2015), pp. 1–31.

26 G. Jeschke and Y. Polyhach, Phys. Chem. Chem. Phys. **9**, 1895 (2007).

27 A. Milov, K. Salikhov, and M. Shirov, Fiz Tverd Tela **23**, 957 (1981).

28 M. Pannier, S. Veit, A. Godt, G. Jeschke, and H.. Spiess, J. Magn. Reson. **142**, 331 (2000).

29 K. Salikhov, I. Khairuzhdinov, and R. Zaripov, Appl. Magn. Reson. **45**, 573 (2014).

30 G. Jeschke, G. Panek, A. Godt, A. Bender, and H. Paulsen, Appl. Magn. Reson. **26**, 223 (2004).

31 G. Jeschke, V. Chechik, P. Ionita, A. Godt, H. Zimmermann, J. Banham, C.R. Timmel, D. Hilger, and H. Jung, Appl. Magn. Reson. **30**, 473 (2006).

32 R.A. Stein, A.H. Beth, and E.J. Hustedt, Methods Enzymol. **563**, 531 (2015).

33 Y.-W. Chiang, P.P. Borbat, and J.H. Freed, J. Magn. Reson. **172**, 279 (2005).

34 Y.-W. Chiang, P.P. Borbat, and J.H. Freed, J. Magn. Reson. **177**, 184 (2005).

35 A. Potapov, Y. Song, T. Meade, D. Goldfarb, A. Astashkin, and A. Raitsimring, J. Magn. Reson. **205**, 38 (2010).

36 M. Ramirez-Cohen, V. Frydman, P. Milko, M.A. Iron, E.H. Abdelkader, M.D. Lee, J.D. Swarbrick, A. Raitsimring, G. Otting, and B. Graham, Phys. Chem. Chem. Phys. **18**, 12847 (2016).

37 E.H. Abdelkader, M.D. Lee, A. Feintuch, M. Ramirez-Cohen, J.D. Swarbrick, G. Otting, B. Graham, and D. Goldfarb, J. Phys. Chem. Lett. **6**, 5016 (2015).

38 H.Y.V. Ching, P.D. Drouhard, H.C. Bertrand, C. Policar, L.C. Tabares, and S. Un, Phys. Chem. Chem. Phys. (2015).

39 A. Feintuch, G. Otting, and D. Goldfarb, in *Methods Enzymol.*, edited by Peter Z. Qin and Kurt Warncke (Academic Press, 2015), pp. 415–457.

40 A. Raitsimring, A. Astashkin, O. Poluektov, and P. Caravan, Appl. Magn. Reson. **28**, 281 (2005).

41 A.M. Raitsimring, A.V. Astashkin, and P. Caravan, in *High Resolut. EPR*, edited by G. Hanson and L.J. Berliner (Springer US, New York, 2009), pp. 581–621.

42 A. Doll, M. Qi, A. Godt, and G. Jeschke, J. Magn. Reson. **273**, 73 (2016).

43 H.J. Hogben, M. Krzystyniak, G.T.P. Charnock, P.J. Hore, and I. Kuprov, J. Magn. Reson. **208**, 179 (2011).

44 D.R. Lide, editor , *CRC Handbook of Chemistry and Physics*, 85th ed. (CRC Press, 2004).

45 A. Abragam and B. Bleaney, *Electron Paramagnetic Resonance of Transition Metal Ions* (Clarendon Press, Oxford, 1970).

46 R.A. Fields and C.A. Hutchison Jr, J. Chem. Phys. **82**, 1711 (1985).

47 W. Low, in *Solid State Phys.*, edited by F. Seitz and D. Turnbull (Academic Press, 1960), pp. 8–75.

48 E. Meirovitch and R. Poupko, J. Phys. Chem. **82**, 1920 (1978).

49 G. Jeschke and H.W. Spiess, in *Nov. NMR EPR Tech.* (Springer, 2006), pp. 21–63.

50 P.P. Borbat and J.H. Freed, in *Struct. Inf. Spin-Labels Intrinsic Paramagn. Cent. Biosci.*, edited by C.R. Timmel and J. Harmer (Springer Berlin Heidelberg, Berlin, 2013), pp. 1–82.

51 A. Borel, H. Kang, C. Gateau, M. Mazzanti, R.B. Clarkson, and R.L. Belford, J. Phys. Chem. A **110**, 12434 (2006).

52 D. Banerjee, H. Yagi, T. Huber, G. Otting, and D. Goldfarb, J. Phys. Chem. Lett. **3**, 157 (2012).

53 S. Rast, A. Borel, L. Helm, E. Belorizky, P.H. Fries, and A.E. Merbach, J. Am. Chem. Soc. **123**, 2637 (2001).

54 A. Borel, S. Laus, A. Ozarowski, C. Gateau, A. Nonat, M. Mazzanti, and L. Helm, J. Phys. Chem. A **111**, 5399 (2007).

55 B. Graham, C.T. Loh, J.D. Swarbrick, P. Ung, J. Shin, H. Yagi, X. Jia, S. Chhabra, N. Barlow, G. Pinta-cuda, T. Huber, and G. Otting, Bioconjug. Chem. **22**, 2118 (2011).
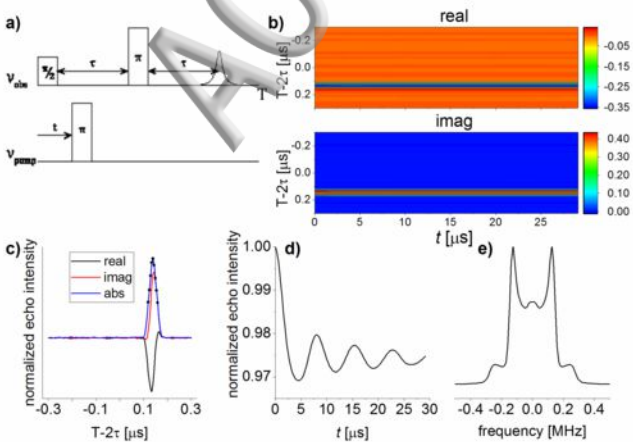
[56] A.V. Astashkin, A.M. Raitsimring, and P. Caravan, J. Phys. Chem. A **108**, 1990 (2004).

[57] V. Lebedev, USSR Comput. Math. Math. Phys. **15**, 44 (1975).

[58] M. Edén and M.H. Levitt, J. Magn. Reson. **132**, 220 (1998).

[59] J.E. Lovett, B.W. Lovett, and J. Harmer, J. Magn. Reson. **223**, 98 (2012).

[60] M. Edén, Y.K. Lee, and M.H. Levitt, J. Magn. Reson. A **120**, 56 (1996).

[61] I.M. Haies, J.A. Jarvis, H. Bentley, I. Heinmaa, I. Kuprov, P.T. Williamson, and M. Carravetta, Phys. Chem. Chem. Phys. **17**, 6577 (2015).

[62] S. Stoll and A. Schweiger, J. Magn. Reson. **178**, 42 (2006).

[63] D. Goldfarb, Phys. Chem. Chem. Phys. **16**, 9685 (2014).

[64] I. Kaminker, H. Yagi, T. Huber, A. Feintuch, G. Otting, and D. Goldfarb, Phys. Chem. Chem. Phys. **14**, 4355 (2012).

[65] A. Doll, M. Qi, N. Wili, S. Pribitzer, A. Godt, and G. Jeschke, J. Magn. Reson. **259**, 153 (2015).

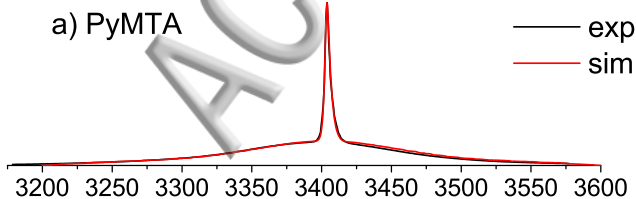a) ν_{obs} — $\frac{\pi}{2}$ — τ — π — τ —

ν_{pump} — t — π

b) real

imag

c)
- real
- imag
- abs

d)

e)

a) PyMTA

b) DOTA

exp
sim

B_0 [mT]

$\Delta\nu=106$ MHz

exp

sim,
$\hat{A}+\hat{B}$ dipolar

sim, $\hat{A}$ dipolar

$\Delta\nu=363$ MHz

exp

sim

$\Delta\nu=469$ MHz

exp

sim

$\Delta\nu=747$ MHz

exp

sim

$\Delta\nu=1090$ MHz

exp

sim

$\Delta\nu=728$ MHz
(K_a)

exp

sim

*

frequency [MHz] r [nm]

r = 2.2 nm

*D*_c [MHz]

2000
1500
1250
1100
950
800
650
500

r = 3 nm

r = 4 nm

frequency [MHz]

r [nm]